Etin Diah Permanasari, Ph.D, Apt.-Role of N-terminal extension of Bacillus stearothermophilus RNase H2 and C-terminal extension of Thermotoga maritima RNase H2

by Etin Diah Permanasari, Ph.d, Apt. Uploaded By Risna

Submission date: 29-Nov-2020 05:33PM (UTC+0700)
Submission ID: 1459070524
File name: febs.12479_-_Etin_Diah.pdf (828.16K)
Word count: 10313
Character count: 52810

the FEBS Journal

Role of N-terminal extension of *Bacillus stearothermophilus* RNase H2 and C-terminal extension of *Thermotoga maritima* RNase H2

Etin-Diah Permanasari[1], Clement Angkawidjaja[1,2], Yuichi Koga[1] and Shigenori Kanaya[1]

1 Department of Material and Life Science, Graduate School of Engineering, Osaka University, Japan
2 International College, Osaka University, Japan

Keywords
junction ribonuclease; RNA DNA hybrid; RNase H; stability; substrate binding

Correspondence
S. Kanaya, Department of Material and Life Science, Graduate School of Engineering, Osaka University, 2-1, Yamadaoka, Suita, Osaka 565-0871, Japan
Tel/Fax: +81 6 6879 7938
E-mail: kanaya@mls.eng.osaka-u.ac.jp

(Received 2 June 2013, revised 1 August 2013, accepted 7 August 2013)

doi:10.1111/febs.12479

Bacillus stearothermophilus RNase H2 (BstRNH2) and *Thermotoga maritima* RNase H2 (TmaRNH2) have N-terminal and C-terminal extensions, respectively, as compared with *Aquifex aeolicus* RNase H2 (AaeRNH2). To analyze the role of these extensions, BstRNH2 and TmaRNH2 without these extensions were constructed, and their biochemical properties were compared with those of their intact partners and AaeRNH2. The far-UV CD spectra of all proteins were similar, suggesting that the protein structure is not significantly altered by removal of these extensions. However, both the junction ribonuclease and RNase H activities of BstRNH2 and TmaRNH2, as well as their substrate-binding affinities, were considerably decreased by removal of these extensions. The stability of BstRNH2 and TmaRNH2 was also decreased by removal of these extensions. The activity, substrate binding affinity and stability of TmaRNH2 without the C-terminal 46 residues were partly restored by the attachment of the N-terminal extension of BstRNH2. These results suggest that the N-terminal extension of BstRNH2 functions as a substrate-binding domain and stabilizes the RNase H domain. Because the C-terminal extension of TmaRNH2 assumes a helix hairpin structure and does not make direct contact with the substrate, this extension is probably required to make the conformation of the substrate-binding site functional. AaeRNH2 showed comparable junction ribonuclease activity to those of BstRNH2 and TmaRNH2, and was more stable than these proteins, indicating that bacterial RNases H2 do not always require an N-terminal or C-terminal extension to increase activity, substrate-binding affinity, and/or stability.

Introduction

RNase H (EC 3.1.26.4) specifically cleaves the RNA strand of RNA·DNA hybrids in the presence of divalent metal ions, such as Mg^{2+} and Mn^{2+}, to yield oligonucleotides with 3′-hydroxyl and 5′-phosphate

Abbreviations
AaeRNH2, *Aquifex aeolicus* RNase H2; BstN, N-terminal 59 residues of *Bacillus stearothermophilus* RNase H2; BstN–TmaRNH2ΔC, *Thermotoga maritima* RNase H2 without the C-terminal 46 residues with the N-terminal 59 residues of *Bacillus stearothermophilus* RNase H2 attached at the N-terminus; BstRNH2, *Bacillus stearothermophilus* RNase H2; BstRNH2ΔN, *Bacillus stearothermophilus* RNase H2 without the N-terminal 59 residues; D15-R1-D13/D29, 29-bp DNA_{15}-RNA_1-DNA_{13}/DNA duplex; HBD, hybrid binding domain; PDB, Protein Data Bank; R12/D12, 12-bp RNA·DNA hybrid; RU, resonance units; TBP, TATA-box binding protein; T_m, melting temperature (temperature at the midpoint of the thermal denaturation transition); TmaRNH2, *Thermotoga maritima* RNase H2; TmaRNH2ΔC, *Thermotoga maritima* RNase H2 without the C-terminal 46 residues; ΔH_m, enthalpy change of unfolding at the melting temperature. ΔS_m, entropy change of unfolding at the melting temperature.

termini [1]. This cleavage occurs via a two-metal-ion catalysis mechanism, in which metal ion A activates the attacking nucleophile, metal ion B destabilizes the enzyme–substrate complex, and both metal ions stabilize the transition state and facilitate product release [2–4]. These metal ions are coordinated by the four acidic active site residues, which are fully conserved in various RNases H [5], except for metagenome-derived LC9-RNase H1 and its homologs, in which the fourth acidic active site residue is replaced by asparagine [6].

RNase H is widely present in bacteria, archaeons, eukaryotes, and retroviruses [5]. On the basis of the differences in their amino acid sequences, RNases H are classified into two major families, type 1 and type 2 RNases H, which are evolutionarily unrelated [5,7]. Type 1 RNases H include RNases H1 and viral RNases H (the C-terminal RNase H domain of reverse transcriptase), and type 2 RNases H include RNases H2 and H3. These RNases H are involved in DNA replication, repair, and transcription [8–14]. Mutations of human RNase H2 cause a severe neurological dysfunction termed Aicardi–Goutières syndrome [15]. Because viral RNase H is required for proliferation of retroviruses, including HIV-1, it is regarded as a target for AIDS therapy [16].

RNase H2 can cleave at the 5′-side of a ribonucleotide when in a duplex either as a single ribonucletotide [17–21] or when attached to a downstream DNA, such as seen in Okazaki primers [22,23]. This activity, termed junction ribonuclease (JRNase) activity, distinguishes it from RNase H1, retroviral RNase H, and RNase H3, although the inability [18,24] and ability [25,26] of RNase H3 to hydrolyze single ribonucleotides in duplex DNA have been reported. The specific contacts between the protein (conserved tyrosine and GRG residues) and the 2′-OH groups of RNA, and distortion of the nucleic acid backbone at the (5′) RNA–DNA(3′) junction, are required for JRNase activity [17]. In contrast, four or five consecutive [2,27] or nonconsecutive [28] contacts between the protein and 2′-OH groups of the RNA strand are required for RNase H activity to cleave RNA·DNA hybrids.

Bacterial RNases H2 are functional in a monomeric form [7], unlike eukaryotic RNases H2, which are functional in a heterotrimeric form [29–31]. Comparison of the amino acid sequences of bacterial RNases H2 indicates that some of them have a relatively long N-terminal or C-terminal extension, but none has both (Fig. S1). For example, *Bacillus stearothermophilus* RNase H2 (BstRNH2) and *Thermotoga maritima* RNase H2 (TmaRNH2) have an N-terminal and a C-terminal extension, respectively, whereas *Aquifex aeolicus* RNase H2 (AaeRNH2) does not have these extensions. Then, the question arises of whether these extensions are structurally and/or functionally important for these RNases H2.

In this study, we constructed a BstRNH2 derivative without an N-terminal extension (BstRNH2ΔN) and an TmaRNH2 derivative without a C-terminal extension (TmaRNH2ΔC), and compared their biochemical properties with those of their intact partners and AaeRNH2. We also constructed and characterized a fusion protein, termed BstN–TmaRNH2ΔC, in which the N-terminal extension of BstRNH2 (BstN) is attached to the N-terminus of TmaRNH2ΔC. On the basis of these results, we discuss the role of BstN and the C-terminal extension of TmaRNH2.

Results

Protein preparation

BstRNH2 and TmaRNH2 have an N-terminal extension of 59 residues (Met1–Leu59) and a C-terminal extension of 45 residues (Asp194–Ile238), respectively, as compared with AaeRNH2 (Fig. 1). According to the crystal structure of TmaRNH2, which is the only structure available for bacterial RNases H2 and has been determined both in a substrate-free form [Protein Data Bank (PDB) code 2ETJ] and in a substrate-bound form [17], the C-terminal extension of TmaRNH2 assumes a relatively independent helix hairpin structure (helices I and J) (Fig. 2). To analyze the role of these extensions, BstRNH2ΔN (Met60–Asn259) and TmaRNH2ΔC (Met1–Leu192) without these extensions were constructed.

BstRNH2ΔN and TmaRNH2ΔC, as well as their intact partners, were overproduced in *Escherichia coli* MIC2067(DE3) lacking the *rnhA* and *rnhB* genes, to avoid contamination by host-derived RNases H1 and H2. AaeRNH2, which consists of 196 residues, was also overproduced in this strain to examine whether it shows similar enzymatic activities to those of BstRNH2ΔN and TmaRNH2ΔC. AaeRNH2 has amino acid sequence identities of 41.0% with BstRNH2ΔN and 46.8% with TmaRNH2ΔC. Upon overproduction, all proteins accumulated in *E. coli* cells in a soluble form, and they were purified to give a single band on SDS/PAGE (Fig. S2). The amount of protein purified from 1 L of culture was ~ 1 mg for BstRNH2 and BstRNH2ΔN, 10 mg for TmaRNH2, 7 mg for TmaRNH2ΔC, and 2 mg for AaeRNH2. The molecular masses were estimated to be 31 kDa for BstRNH2, 24 kDa for BstRNH2ΔN, 27 kDa for TmaRNH2, 21 kDa for TmaRNH2ΔC, and 22 kDa for AaeRNH2, by gel filtration chromatography. These values are comparable to those calculated

Fig. 1. Alignment of the amino acid sequences. The amino acid sequences of BstRNH2 (Bst), TmaRNH2 (Tma) and AaeRNH2 (Aae) are compared. The accession numbers are BAB91155 for BstRNH2, AAD35996 for TmaRNH2, and AAC07736 for AaeRNH2. The ranges of the secondary structures of TmaRNH2 are shown above the sequences. The residues that are conserved in at least two different proteins are highlighted in black. The active site residues are indicated by the filled circles above the sequences. The residues of TmaRNH2 that contact the 2′-OH group of the single ribonucleotide of the substrate (conserved Tyr and the residues forming a GRG motif) are indicated by the stars. Gaps are denoted by dashes. The numbers represent the positions of the amino acids relative to the initiator Met for each protein. BstN and the C-terminal 46 residues of TmaRNH2, which are truncated to construct BstRNH2ΔN and TmaRNH2ΔC, respectively, are boxed.

from the amino acid sequences (28 892 Da for BstRNH2, 21 608 Da for BstRNH2ΔN, 26 630 Da for TmaRNH2, 21 115 Da for TmaRNH2ΔC, and 22 045 Da for AaeRNH2), suggesting that these proteins exist as monomers in solution.

CD spectra

The far-UV and near-UV CD spectra of the proteins were measured at 25 °C and pH 8.0, and are compared in Fig. 3A,B. The far-UV CD spectra reveal the secondary structures of the proteins, whereas the near-UV CD spectra reveal the local conformation around the aromatic residues, such as tryptophan and tyrosine. The far-UV CD spectra of BstRNH2ΔN and TmaRNH2ΔC were similar to those of their intact partners, although these spectra had a shallower trough at 210–220 nm than the spectra of their intact partners. The near-UV CD spectrum of TmaRNH2ΔC was also similar to that of TmaRNH2. In contrast, the near-UV CD spectrum of BstRNH2ΔN was different from that of BstRNH2. These results suggest that removal of the N-terminal and C-terminal extensions does not seriously affect the overall structures of BstRNH2 and TmaRNH2, respectively. The near-UV CD spectrum of BstRNH2 was changed by removal of BstN, probably because the environment of the aromatic residues located near the interface between the deleted region and the RNase H domain was altered. According to a 3D model of BstRNH2ΔN, two tyrosines (Tyr67 and Tyr101) are located near the position where the N-terminal residue is located (Fig. S3). These residues, as well as two tryptophans (Trp24 and Trp56) in the deleted region, are candidates for the aromatic residues located near the interface. According to the crystal structure of TmaRNH2, no tryptophans or tyrosines are located at and around the deleted region.

The far-UV CD spectra of BstRNH2ΔN, TmaRNH2ΔC and AaeRNH2 were similar, suggesting

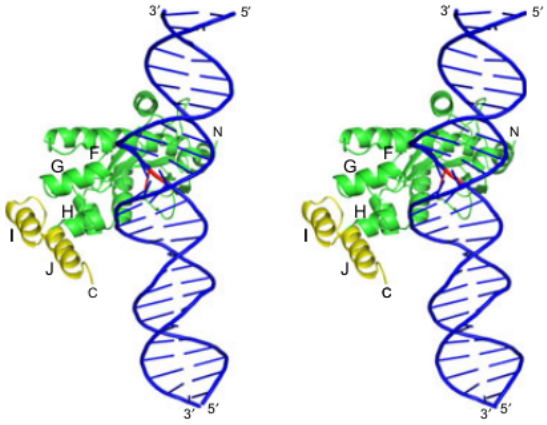

Fig. 2. C-terminal helix hairpin structure of TmaRNH2. A stereoview of the 3D model of TmaRNH2 in complex with 29 bp dsDNA containing single ribonucleotide (D15-R1-D13/D29) is shown in blue and red, respectively. The C-terminal helix hairpin structure truncated to construct TmaRNH2ΔC (Thr193–Phe238) is shown in yellow. Helices F–J, which constitute the C-terminal domain of TmaRNH2, are indicated. 'N' and 'C' represent the N-termini and C-termini, respectively.

but they share a main-chain fold. In contrast, the near-UV CD spectra of these proteins were different, suggesting that the local conformations around the aromatic residues of these proteins are different. BstRNH2ΔN and TmaRNH2ΔC do not contain a tryptophan, but contain nine and four tyrosines, respectively. AaeRNH2 contains one tryptophan and nine tyrosines. Only two tyrosines are conserved in these proteins. These differences may account for the difference in their near-UV CD spectra.

Enzymatic activities

The JRNase and RNase H activities of all proteins were determined at 30 °C with a 29-bp DNA_{15}-RNA_1-DNA_{13}/DNA duplex (D15-R1-D13/D29) and a 12-bp RNA·DNA hybrid (R12/D12), respectively, as substrate. Manganese and magnesium ions were used as metal cofactors. All proteins examined cleaved the D15-R1-D13/D29 substrate almost exclusively at the (5′)DNA–RNA(3′) junction, regardless of the metal cofactor (Fig. 4A). In contrast, BstRNH2, TmaRNH2 and AaeRNH2 cleaved the R12/D12 substrate at multiple sites with different sequence preferences (Fig. 4B). The preferred cleavage sites of this substrate with TmaRNH2 were not significantly changed when the metal cofactor was changed, and were comparable to those with TmaRNH2ΔC. In contrast, the preferred cleavage sites of this substrate with BstRNH2 were slightly changed when the metal cofactor was changed, and were different from those with BstRNH2ΔN. The preferred cleavage sites of this substrate with AaeRNH2 were also slightly changed when the metal cofactor was changed. These results indicate that the sequence preference of TmaRNH2 is not significantly changed by removal of the C-terminal extension, whereas that of BstRNH2 is changed by removal of BstN.

The specific JRNase and RNase H activities of the proteins were determined by quantifying the amount of the substrate and products separated on urea gel. For simplicity, the JRNase and RNase H activities determined in the presence of Mn^{2+} and Mg^{2+} are termed $JRNase^{Mn}$, $JRNase^{Mg}$, $RNase\ H^{Mn}$ and $RNase\ H^{Mg}$ activities. The optimum concentrations

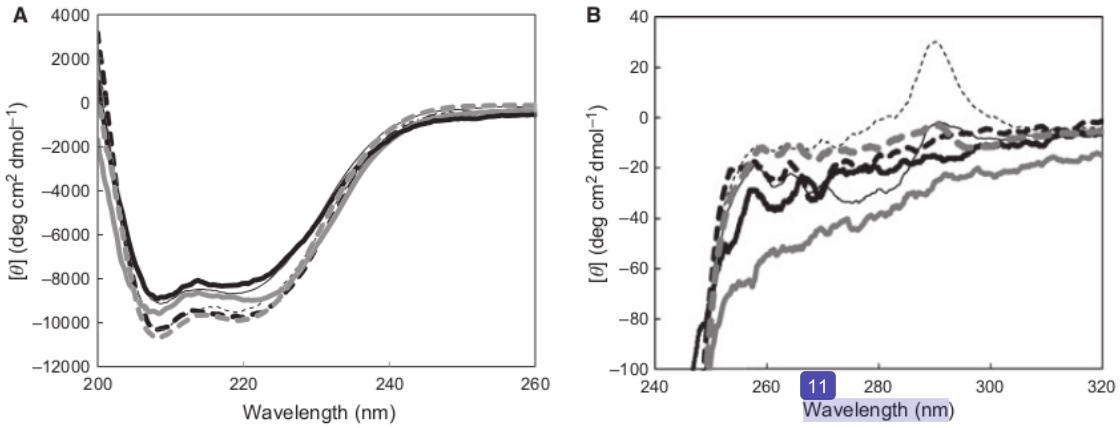

Fig. 3. CD spectra. The far-UV (A) and near-UV (B) CD spectra of BstRNH2 (thin dashed dark line), BstRNH2ΔN (thin solid dark line), TmaRNH2 (thick dashed dark line), TmaRNH2ΔC (thick solid dark line), AaeRNH2 (solid gray line) and BstN–TmaRNH2ΔC (dashed gray line) are shown. These spectra were obtained at 25 °C, as described in Experimental procedures.

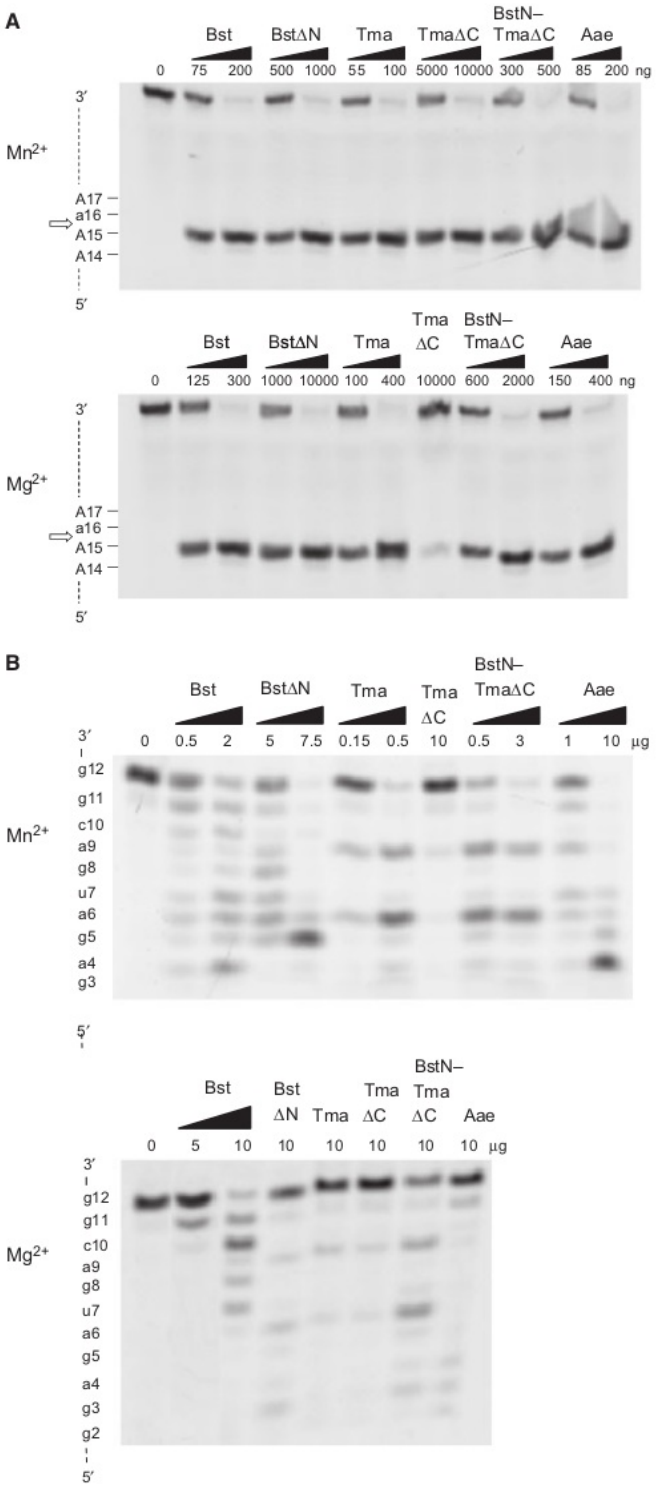

Fig. 4. Cleavage of oligomeric substrates by various RNases H. The 5′-end-labeled DNA_{15}-RNA_1-DNA_{13}/DNA_{29} (A) and RNA_{12}/DNA_{12} (B) were hydrolyzed by the enzyme in the presence of either Mn^{2+} or Mg^{2+} at 30 °C for 15 min, and the hydrolysates were separated on a 20% polyacrylamide gel containing 7 M urea, as described in Experimental procedures. The reaction volume was 10 μL, and concentration of the substrate was 1.0 μM. The sequences of DNA_{15}-RNA_1-DNA_{13} and RNA_{12} around the cleavage sites are indicated along the gel. Deoxyribonucleotides are indicated by uppercase letters, and ribonucleotides are indicated by lowercase letters. Enzymes: Bst, BstRNH2; BstΔN, BstRNH2ΔN; Tma, TmaRNH2; TmaΔC, TmaRNH2ΔC; BstN–TmaΔC, BstN–TmaRNH2ΔC; Aae, AaeRNH2. The major site of cleavage of DNA_{15}-RNA_1-DNA_{13} by these enzymes is shown by an arrow. The cleavage sites of RNA_{12} are not shown, because this oligonucleotide is cleaved by these enzymes at all possible sites between g2 and g12.

of the metal ions for these activities were 10 mM for BstRNH2ΔN, BstRNH2, and AaeRNH2, and 1 mM for TmaRNH2ΔC and TmaRNH2, regardless of the metal cofactor (data not shown). The maximal specific JRNase^{Mn}, JRNase^{Mg}, RNase H^{Mn} and RNase H^{Mg} activities of these proteins are summarized in Table 1.

When the four activities mentioned above were compared for BstRNH2, TmaRNH2, and AaeRNH2, the JRNase^{Mn} activity was always the highest, and other activities decreased in the order JRNase^{Mn} > JRNase^{Mg} > RNase H^{Mn} > RNase H^{Mg}. However, the JRNase^{Mg} activity was lower than the JRNase^{Mn} activity by only 40–50% for these proteins. In contrast, the RNase H^{Mg} activity was lower than the RNase H^{Mn} activity by 10-fold for BstRNH2, 100-fold for TmaRNH2, and 50-fold for AaeRNH2. These results indicate that BstRNH2, TmaRNH2 and AaeRNH2 show a weak preference for Mn^{2+} for JRNase activity and a strong preference for Mn^{2+} for RNase H activity. In addition, The RNase H^{Mn} activity was lower than the JRNase^{Mg} activity by four-fold for BstRNH2, 1.5-fold for TmaRNH2, and seven-fold for AaeRNH2, indicating that these proteins prefer the D15-R1-D13/D29 substrate to the R12/D12 substrate. Similar results have been reported for TmaRNH2, except that it shows a weak preference for Mg^{2+}, instead of Mn^{2+}, for JRNase activity [17]. This discrepancy is probably caused by the difference in the substrate used for assay.

When the four activities of BstRNH2ΔN were compared with those of BstRNH2, they were reduced by seven-fold for JRNase^{Mn} activity, 40-fold for JRNase^{Mg} activity, 10-fold for RNase H^{Mn} activity, and nine-fold for RNase H^{Mg} activity. These results indicate that BstN is important for activity, especially for JRNase^{Mg} activity. When the four activities of TmaRNH2ΔC were compared with those of TmaRNH2, they were reduced by 90-fold for JRNase^{Mn} activity, 440-fold for JRNase^{Mg} activity, 500-fold for RNase H^{Mn} activity, and seven-fold for RNase H^{Mg} activity. These results indicate that the C-terminal extension of TmaRNH2 is important for activity, especially for JRNase^{Mn}, JRNase^{Mg} and RNase H^{Mn} activities.

Complementation of the temperature-sensitive (ts) growth phenotype of an RNase H-deficient *E. coli* strain

E. coli MIC2067(DE3) shows an RNase H-dependent temperature-sensitive (ts) growth phenotype [32]. To examine whether BstRNH2, BstRNH2ΔN, TmaRNH2, TmaRNH2ΔC and AaeRNH2 complement this phenotypic defect, *E. coli* MIC2067(DE3) transformants for overproduction of these proteins were grown on LB-agar plates containing 30 mg·L^{-1} chloramphenicol and 50 mg·L^{-1} ampicillin in the absence of isopropyl thio-β-D-galactoside at permissive (30 °C) and nonpermissive (42 °C) temperatures. *E. coli* transformants for overproduction of BstRNH2 and TmaRNH2 formed colonies on these plates at both 30 °C and 42 °C, whereas those for overproduction of other proteins formed colonies only at 30 °C (data not shown). These results indicate that BstRNH2 and TmaRNH2 complement the ts phenotype of *E. coli* MIC2067(DE3), whereas the other three proteins do not. Because the JRNase activity of AaeRNH2 was comparable to that of BstRNH2 regardless of the metal cofactor (Table 1), the RNase H activities of BstRNH2ΔN, TmaRNH2ΔC and AaeRNH2 are probably too low to complement the ts phenotype of *E. coli* MIC2067(DE3). It seems possible, but unlikely, that the production levels of

Table 1. Specific activities of the proteins. Hydrolysis of the D15-R1-D13/D29 (for JRNase activity) and R12/D12 (for RNase H activity) substrates by the protein was performed at 30 °C under the conditions described in Experimental procedures. The $MnCl_2$ and $MgCl_2$ concentrations were 1 mM for TmaRNH2 and TmaRNH2ΔC, and 10 mM for other proteins, regardless of the metal ions. Experiments were carried out at least twice, and the average values are shown together with the errors. The specific activities of the proteins relative to the JRNase^{Mn} activity of TmaRNH2 are shown. The specific JRNase^{Mn}, JRNase^{Mg}, RNase H^{Mn} and RNase H^{Mg} activities of the mutant proteins (TmaRNH2ΔC, BstN–TmaRNH2ΔC, and BstRNH2ΔN) relative to those of the parent proteins are shown in parentheses.

Protein	JRNase^{Mn} activity (unit/mg)	Relative activity (%)	JRNase^{Mg} activity (unit/mg)	Relative activity (%)	RNase H^{Mn} activity (unit/mg)	Relative activity (%)	RNase H^{Mg} activity (unit/mg)	Relative activity (%)
TmaRNH2	6.2 ± 0.44	100	3.4 ± 0.047	55	2.2 ± 0.094	35	0.022 ± 0.0002	0.35
TmaRNH2ΔC	0.070 ± 0.0030	1.1	0.0077 ± 0.0013	0.12 (0.23)	0.0044 ± 0.0012	0.070 (0.20)	0.0033 ± 0.0009	0.053 (15)
BstN–TmaRNH2ΔC	1.2 ± 0.047	19	0.56 ± 0.008	9.0 (16)	0.65 ± 0.028	10 (29)	0.025 ± 0.0028	0.40 (110)
BstRNH2	4.7 ± 0.15	76	2.7 ± 0.037	44	0.67 ± 0.019	11	0.067 ± 0.003	1.1
BstRNH2ΔN	0.69 ± 0.019	11 (15)	0.068 ± 0.001	1.1 (2.5)	0.070 ± 0.004	1.1 (10)	0.0071 ± 0.0012	0.11 (11)
AaeRNH2	4.3 ± 0.29	69	2.4 ± 0.16	39	0.33 ± 0.005	5.3	0.0092 ± 0.0011	0.15

these proteins are too low to complement this phenotype, because the production levels of these proteins upon induction for overproduction were comparable to or rather higher than that of BstRNH2 (data not shown).

Binding to substrate

To examine whether removal of BstN and the C-terminal extension of TmaRNH2 affects the substrate binding, the binding affinities of BstRNH2, BstRNH2ΔN, TmaRNH2 and TmaRNH2ΔC for the D15-R1-R13/D29 substrate were analyzed in the absence of the metal cofactor, with surface plasmon resonance (Biacore system). These proteins were injected onto the sensor chip, on which the D15-R1-D13/D29 substrate was immobilized. When 1 μM BstRNH2 or TmaRNH2 was injected onto the sensor chip, a significant increase in resonance units (RU) was detected (Fig. 5). In contrast, only a slight increase in RU was detected when 1 μM BstRNH2ΔN or TmaRNH2ΔC was injected. The association constants, K_A, of these proteins for binding to the substrate, which were determined by measuring the equilibrium binding responses at various concentrations of the proteins, are summarized in Table 2. The K_A values of BstRNH2ΔN and TmaRNH2ΔC were lower than those of BstRNH2 and TmaRNH2 by ~ 30-fold and > 100 fold, respectively. These results indicate that removal of BstN and the C-terminal extension of TmaRNH2 greatly reduces the binding affinities of these proteins for the substrate.

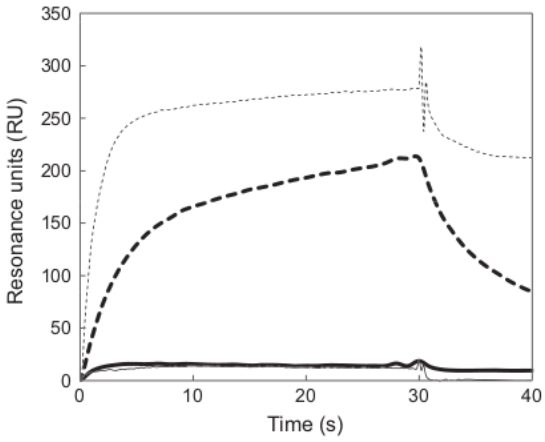

Fig. 5. Binding of the proteins to immobilized dsDNA with a single ribonucleotide. The sensorgrams showing the binding of 1 μM BstRNH2 (thin dashed line), BstRNH2ΔN (thin solid line), TmaRNH2 (thick dashed line) and TmaRNH2ΔC (thick solid line) to the immobilized D15-R1-D13/D29 substrate are shown. Injections were performed at time zero for 30 s.

Thermal stability

To examine whether removal of BstN and the C-terminal extension of TmaRNH2 affects protein stability, the thermal stabilities of BstRNH2, BstRNH2ΔN, TmaRNH2 and TmaRNH2ΔC were analyzed by monitoring changes in the CD values at 222 nm. The thermal stability of AaeRNH2 was also analyzed, for comparative purpose. In the presence of 1.5 M guanidine hydrochloride at pH 8.0, all proteins unfolded in a single cooperative fashion in a reversible manner. The thermal denaturation curves of these proteins are compared in Fig. 6. The parameters characterizing the thermal denaturation of these proteins are summarized in Table 3. Comparison of these parameters indicated that BstRNH2ΔN and TmaRNH2ΔC were less stable than their intact partners by 11.2 °C and 19.5 °C in melting temperature (temperature at the midpoint of the thermal denaturation transition) (T_m), respectively. The enthalpy change of unfolding at T_m (ΔH_m) and the entropy change of unfolding at T_m (ΔS_m) values of these proteins were also decreased as compared with those of their intact partners. These results indicate that BstN and the C-terminal extension of TmaRNH2 greatly contribute to protein stabilization. Comparison of the T_m values of AaeRNH2, TmaRNH2 and BstRNH2 indicated that the stability of these proteins decreased in this order. AaeRNH2 was more stable than TmaRNH2 and BstRNH2 by 10.1 °C and 24.9 °C in T_m, respectively. The upper limits of the growth temperatures of *A. aeolicus*, *T. maritima* and *B. stearothermophilus* are 95 °C [33], 90 °C [34], and

Table 2. Association constants of the proteins for substrate binding. Binding of the proteins to the D15-R1-D13/D29 substrate immobilized on the sensor chip was analyzed in the absence of the metal cofactor by surface plasmon resonance, as described in Experimental procedures. The K_A values of the proteins relative to that of BstRNH2 are shown. The K_A values of TmaRNH2ΔC and BstN–TmaRNH2ΔC relative to that of TmaRNH2 are shown in parentheses.

Protein	K_A (M^{-1}) × 10^{-5}	Relative K_A (%)
BstRNH2	190	100
BstRNH2ΔN	6.1	3.2
TmaRNH2	3.4	1.8
TmaRNH2ΔC	< 0.03	< 0.02 (< 0.9)
BstN–TmaRNH2ΔC	10	5.3 (290)
AaeRNH2	3.9	2.1

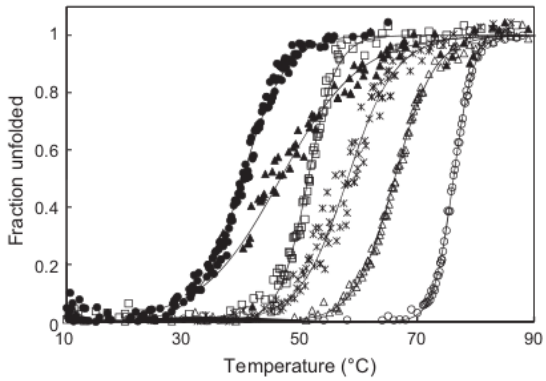

Fig. 6. Thermal denaturation curves. Thermal denaturation curves of AaeRNH2 (open circles), TmaRNH2 (open triangles), TmaRNH2ΔC (closed triangles), BstRNH2 (open squares), BstRNH2ΔN (closed circles) and BstN–TmaRNH2ΔC (stars) are shown. These curves were obtained at pH 8.0 in the presence of 1.5 M guanidine hydrochloride, as described in Experimental procedures. The theoretical curves are drawn on the assumption that the proteins are denatured via a two-state mechanism.

70 °C [35], respectively. Thus, the stability of these proteins decreased in proportion to the growth temperatures of their source organisms. Note that the ΔH_m values of AaeRNH2, BstRNH2, and TmaRNH2, as well as their ΔS_m values, decreased in the same order. The reason why these values did not decrease in proportion to their T_m values remains to be clarified.

Biochemical properties of TmaRNH2ΔC with BstN attached at the N-terminus (BstN–TmaRNH2ΔC)

To examine whether BstN restores the activity and stability of TmaRNH2ΔC, BstN–TmaRNH2ΔC, in which BstN is attached to the N-terminus of TmaRNH2ΔC, was constructed. BstN–TmaRNH2ΔC was overproduced in *E. coli* and purified to give a single band on SDS/PAGE (Fig. S2). The production level and purification yield of BstN–TmaRNH2ΔC were comparable to those of TmaRNH2ΔC. The molecular mass of this protein as estimated with gel filtration chromatography (31 kDa) was comparable to that calculated from the amino acid sequence (28 399), suggesting that it exists as a monomer in solution. The far-UV and near-UV CD spectra of BstN–TmaRNH2ΔC were similar to those of TmaRNH2ΔC (Fig. 3), suggesting that the attachment of BstN did not seriously affect the structure of TmaRNH2ΔC.

When *E. coli* MIC2067(DE3) transformants for overproduction of BstN–TmaRNH2ΔC were grown on LB-agar plates in the absence of isopropyl thio-β-D-galactoside (IPTG), they formed colonies at both 30 °C and 42 °C (data not shown). This result indicates that BstN–TmaRNH2ΔC has the ability to complement the ts phenotype of *E. coli* MIC2067(DE3). Thus, BstN restores the RNase H activity of TmaRNH2ΔC. When the enzymatic activity of BstN–TmaRNH2ΔC was analyzed with the oligomeric substrates, BstN–TmaRNH2ΔC cleaved the D15-R1-D13/D29 and R12/D12 substrates with the same sequence preferences as those of TmaRNH2, regardless of the metal cofactor (Fig. 4). The JRNase^{Mn}, JRNase^{Mg} and RNase H^{Mn} activities of BstN–TmaRNH2ΔC were higher than those of TmaRNH2ΔC by 17-fold, 70-fold, and 150-fold, respectively, and lower than those of TmaRNH2 by five-fold, six-fold, and three-fold, respectively (Table 1). The RNase H^{Mg} activity of BstN–TmaRNH2ΔC was higher than that of TmaRNH2ΔC by eight-fold, and comparable to that of TmaRNH2 (Table 1). These results indicate that BstN at least partly restores the enzymatic activity of TmaRNH2ΔC. When the binding affinity of BstN–TmaRNH2ΔC for the D15-R1-D13/D29 substrate was analyzed in the absence of the metal cofactor, with surface plasmon

Table 3. Parameters characterizing thermal denaturation of the proteins. Parameters characterizing thermal denaturation of the proteins were determined from the thermal denaturation curves shown in Fig. 4. The melting temperature (T_m) is the temperature at the midpoint of the thermal denaturation transition. ΔT_m1 is the difference in T_m between AaeRNH2 and TmaRNH2 or BstRNH2, and is calculated as T_m (TmaRNH2 or BstRNH2) – T_m (AaeRNH2). ΔT_m2 is the difference in T_m between TmaRNH2ΔC or BstN–TmaRNH2ΔC and TmaRNH2, and between BstRNH2ΔN and BstRNH2, and is calculated as T_m (TmaRNH2ΔC or BstN–TmaRNH2ΔC) – T_m (TmaRNH2) or T_m (BstRNH2ΔN) – T_m (BstRNH2). ΔH_m and ΔS_m are the enthalpy and entropy changes of unfolding at T_m calculated by van't Hoff analysis.

Protein	T_m (°C)	ΔT_m1 (°C)	ΔT_m2 (°C)	ΔH_m (kJ mol^{-1})	ΔS_m (kJ mol^{-1}·K^{-1})
AaeRNH2	76.2 ± 0.03	–	–	601.9 ± 8.6	1.7 ± 0.02
TmaRNH2	66.1 ± 0.05	−10.1	–	282.9 ± 5.2	0.8 ± 0.02
TmaRNH2ΔC	46.6 ± 0.81	–	−19.5	125.6 ± 23.9	0.4 ± 0.07
BstN–TmaRNH2ΔC	58.1 ± 0.66	–	−8.0	220.1 ± 41.2	0.7 ± 0.13
BstRNH2	51.3 ± 0.06	−24.9	–	361.1 ± 11.3	1.1 ± 0.03
BstRNH2ΔN	40.1 ± 0.1	–	−11.2	221.9 ± 8.7	0.7 ± 0.03

resonance, it was higher than those of TmaRNH2ΔC and TmaRNH2 by > 300-fold and three-fold in K_A, respectively (Table 2). This result indicates that BstN functions as a potent substrate-binding domain, and restores the substrate-binding affinity of TmaRNH2ΔC beyond the level of TmaRNH2. When the thermal stability of BstN–TmaRNH2ΔC was analyzed in the presence of 1.5 M guanidine hydrochloride by monitoring changes in the CD values at 222 nm, it reversibly unfolded in a single cooperative fashion. The thermal denaturation curve of this protein is shown in Fig. 6. BstN–TmaRNH2ΔC was more stable than TmaRNH2ΔC by 11.5 °C and less stable than TmaRNH2 by 8 °C in T_m (Table 3). This result indicates that BstN partly restores the stability of TmaRNH2ΔC.

Discussion

Role of BstN

The finding that removal of BstN does not significantly affect the structure, but reduces the activity, substrate-binding affinity and stability, of the protein indicates that BstN is important for substrate binding and protein stability. BstN is probably folded into a relatively independent structure, and functions as a substrate-binding domain. BstN is probably kept folded and functions in an isolated form as well, because attachment of BstN to the N-terminus of TmaRNH2ΔC greatly increases the activity and substrate-binding affinity of TmaRNH2ΔC. However, BstN contributes to the stabilization of BstRNH2, suggesting that BstN interacts with the RNase H domain. BstN also contributes to the stabilization of BstN–TmaRNH2ΔC, but less significantly than to the stabilization of BstRNH2, probably because the interactions at the interface between BstN and RNase H domain that contribute to the stabilization of BstRNH2 are only partially conserved in BstN–TmaRNH2ΔC.

It has been reported that BstRNH2ΔN does not bind to RNA·DNA hybrids and therefore does not show RNase H activity in the presence of Mn^{2+} [36]. However, in this study, we demonstrated that BstRNH2ΔN shows RNase H activity in the presence of either Mn^{2+} or Mg^{2+}, although it is lower than that of BstRNH2 by 9 to 10-fold (Table 1). The reason for this discrepancy is not understood. However, BstRNH2ΔN probably retains weak substrate-binding affinity for RNA·DNA hybrids as well, because BstRNH2ΔN retains both weak JRNase activity (Table 1) and weak binding affinity for the D15-R1-D13/D29 substrate (Table 2).

BstRNH2 cleaves the 12-bp R12/D12 substrate (RNase H substrate) preferentially at g11–g12 in the presence of Mg^{2+}, whereas BstRNH2ΔN cleaves it preferentially at the different sites under the same conditions (Fig. 4B). This result suggests that BstN facilitates binding of the substrate to the enzyme in such a way that the scissile phosphate group between g11 and g12 contacts the active site, and the upstream region of this phosphate group of the substrate contacts the interface between the catalytic and C-terminal domains. The structure of this complex is different from that of the complex between the enzyme and the long 29-bp D15-R1-D13/D29 substrate (JRNase substrate), in which the enzyme binds near the center of the substrate. Therefore, the mechanism for stabilization of the complex between the enzyme and R12/D12 substrate by BstN may be different from that of the complex between the enzyme and D15-R1-D13/D29 substrate. However, BstRNH2 shows a weak preference for the R12/D12 substrate (Table 1). Therefore, we discuss the role of BstN on the basis of the JRNase activity of BstRNH2 in this study.

A 3D model of BstRNH2ΔN is highly similar to the crystal structure of TmaRNH2 (Fig. S3), suggesting that BstRNH2 contacts the substrate as does TmaRNH2 (Fig. 2). In Fig. 2, a model of the complex between TmaRNH2 and the 29-bp D15-R1-D13/D29 substrate is shown. This model is constructed on the basis of the crystal structure of TmaRNH2 in complex with the short substrate (12-bp D5-R1-D6/D12) [17]. In this model, the substrate is slightly bent at the position where it contacts the enzyme, owing to the deformation of the nucleic acid backbone at the RNA–DNA junction [17]. BstN probably contacts the noncleaved DNA strand four to six bases away (downstream) from the scissile phosphate group. Further structural studies will be required to understand the mechanism by which BstN binds to the substrate.

Database searches indicate that not only RNases H2 from the genus *Bacillus*, but also those from other genera, such as *Enterococcus*, *Streptococcus*, *Staphylococcus*, *Ruminococcus*, *Blautia*, *Megasphaera*, *Listeria*, and *Clostridium*, have an N-terminal extension (Fig. S1). These extensions show a similarity to BstN both in size (50–60 residues) and amino acid sequence (at least 20%), suggesting that they assume a similar structure as that of BstN and function as substrate-binding domains. It has been reported that almost every eukaryotic RNase H1 and several bacterial RNases H1 have hybrid binding domains (HBDs) at their N-termini, which are important for substrate binding [20,37]. Likewise, bacterial RNases H3 have TATA-box binding protein (TBP)-like domains at their N-termini,

which are important for substrate binding [24,32]. However, none of the N-terminal extensions of bacterial RNases H2 show significant amino acid sequence similarity to HBDs or TBP-like domains, suggesting that their structures are different from those of HBDs and TBP-like domains.

Role of the C-terminal extension of TmaRNH2

According to the crystal structure of the TmaRNH2–substrate complex, TmaRNH2 consists of the catalytic and C-terminal domains, and the substrate binds to a groove on the protein surface between these domains [17]. This interaction is preserved in the model shown in Fig. 2. The C-terminal domain of TmaRNH2 consists of five helices (helices F–J) and mainly contacts the noncleaved strand through van der Waals interactions or interactions mediated by the backbone of the protein. Helices G and H provide a surface that is responsible for binding of the noncleaved strand. In contrast, a helix hairpin structure containing helices I and J, which corresponds to the C-terminal extension, does not contact the substrate. This result suggests that the C-terminal helix hairpin structure is not involved in substrate binding. The previous finding that TmaRNH2 efficiently hydrolyzes the 12-bp D5-R1-D6/D12 substrate [17], which is too short to contact the helix hairpin structure, supports this hypothesis. Nevertheless, removal of this helix hairpin structure greatly reduces the binding affinity for the D15-R1-D13/D29 substrate (Table 2) and both the JRNase and RNase H activities (Table 1). This result suggests that the C-terminal helix hairpin structure is required to make the conformation of the C-terminal domain functional. TmaRNH2ΔC may assume a non-native structure, in which the shape of the surface responsible for binding of the noncleaved strand is slightly changed.

The substrate-binding affinity and activity of TmaRNH2ΔC are partly restored by the attachment of BstN to the N-terminus of TmaRNH2ΔC. The sequence preference of the resultant fusion protein is nearly identical to that of TmaRNH2, indicating that the catalytic domain, instead of BstN, determines the sequence preference. These results suggest that removal of the C-terminal helix hairpin structure causes only a subtle change in the conformation of the C-terminal domain, and this conformational change greatly decreases the interactions between the protein and substrate without significantly altering them. BstN probably stabilizes the protein–substrate complex, which is greatly destabilized by removal of the C-terminal helix hairpin structure. It is unlikely that the structure of TmaRNH2ΔC is restored by the attachment of BstN, because the position of BstN attached to TmaRNH2ΔC is apparently quite different from that of the C-terminal helix hairpin structure (Fig. 2), and the substrate-binding affinity of BstN–TmaRNH2ΔC is three-fold higher than that of TmaRNH2 (Table 2). Removal of the C-terminal helix hairpin structure decreases the conformational stability of the protein as well, suggesting that this structure also contributes to the stabilization of the protein.

Database searches indicate that not only RNases H2 from the genus *Thermotoga*, but also those from other genera, such as *Arthrobacter*, *Comamonas*, *Burkholderia*, *Acidovorax*, *Fervidobacterium*, and *Bradyrhizobium*, have a C-terminal extension (Fig. S1). However, unlike the N-terminal extensions of bacterial RNases H2, these extensions vary in both size and amino acid sequence, suggesting that they have variable structures. Because the catalytic domains of these RNases H2 share a structure with that of TmaRNH2, the C-terminal extensions of these RNases H2 are probably required to make the conformation of the C-terminal domain functional.

Activity and stability of AaeRNH2

AaeRNH2 shows comparable JRNase activity to those of TmaRNH2 and BstRNH2, despite the lack of an N-terminal or C-terminal extension (Table 1). In addition, AaeRNH2 is more stable than TmaRNH2 and BstRNH2. These results indicate that bacterial RNase H2 does not always require an N-terminal or C-terminal extension to increase the activity, substrate-binding affinity, and/or stability. Various RNases H2 from mesophilic and psychrophilic bacteria, such as *E. coli*, *Haemophilus haemolyticus*, and *Shewanella baltica*, contain neither an N-terminal nor a C-terminal extension (Fig. S1), suggesting that efficient functioning without these extensions is not unique to highly thermostable RNases H2.

AaeRNH2 is more stable than TmaRNH2 and BstRNH2 by 10.1 °C and 24.9 °C, respectively, in T_m. It has been reported that hyperthermophilic proteins are stabilized by the combination of various factors, such as an increased number of ion pairs (ion pair networks) [38,39], an increased number of metal-binding sites [40], a reduced cavity volume [41], anchoring of the C-terminal tail [42], increased interior hydrophobicity [43], increased packing density, including aromatic interactions [38], increased molecular compactness [44], oligomerization [45], an increased number of prolines in loop regions [46], and an increased number of disulfide bonds [47]. To understand the stabilization mechanism of AaeRNH2, a 3D

model of this protein was constructed, based on the crystal structure of TmaRNH2. The backbone structure of this model is nearly identical to those of a 3D model of BstRNH2ΔN and a crystal structure of TmaRNH2 (Fig. S3), suggesting that there is little difference in molecular compactness among them. Comparison of these structures indicates that the cavity volume, interior hydrophobicity and the number of prolines in the loop regions do not correlate with the protein stability. For example, the cavity volume, which is calculated with CASTP [48], is 343 Å^3 for AaeRNH2, 80 Å^3 for TmaRNH2, and 289 Å^3 for BstRNH2ΔN. The contents of the buried nonpolar and polar residues are 35.7% and 12.2% for AaeRNH2, 38.7% and 10.5% for TmaRNH2, and 38.0% and 11.0% for BstRNH2ΔN, respectively. The numbers of prolines in loop regions are five for AaeRNH2, two for TmaRNH2, and 10 for BstRNH2ΔN. None of these proteins contains any disulfide bonds or metal ions other than those required for activity. However, the number of ion pairs increases as the protein stability increases. The numbers of ion pairs and ion pair networks, which are calculated on the basis of the assumption that ion pairs are formed between two oppositely charged groups located within a distance of 5 Å, and that ion pair networks are formed by at least four charged residues, are, respectively, 11 and one for AaeRNH2, eight and one for TmaRNH2 without the C-terminal extension region, and six and zero for BstRNH2ΔN. In addition, AaeRNH2 contains four aromatic interactions, whereas TmaRNH2 and BstRNH2ΔN do not contain aromatic interactions. These results suggest that stabilization by ion pairs and aromatic interactions at least partly account for the difference in stability between AaeRNH2 and TmaRNH2 or BstRNH2.

Experimental procedures

Plasmid construction

Plasmids pET800TM and pET600AA for overproduction of TmaRNH2 and AaeRNH2, respectively, were previously constructed in our laboratory [49]. Plasmid pET800BS for overproduction of BstRNH2 was constructed by ligating the *Nde*I–*Sal*I fragment of pJAL800ST [36] containing the BstRNH2 gene into the *Nde*I–*Sal*I sites of pET25b (Novagen, Madison, WI, USA). Plasmids pET670TMΔC and pET620BSΔN for overproduction of TmaRNH2ΔC and BstRNH2ΔN, respectively, were constructed by PCR with the KOD-Plus mutagenesis kit (Toyobo, Kyoto, Japan), according to the manufacturer's instructions. Plasmids pET800TM and pET800BS were used as templates. The mutagenic primers were designed such that the C-terminal 46 residues of TmaRNH2 and BstN are removed. Plasmid pET850BSTMΔC for overproduction of BstN–TmaRNH2ΔC was constructed by the overlap PCR extension method, as described previously for the construction of the plasmid for complementation assay [50]. The DNA oligomers for PCR were synthesized by Hokkaido System Science (Sapporo, Japan). PCR was performed with a GeneAmp PCR system 2400 (Applied Biosystems, Tokyo, Japan). All DNA sequences were confirmed with the ABI Prism 310 DNA sequencer (Applied Biosystems).

Overproduction and purification

E. coli MIC2067(DE3), which lacks the *rnh*A and *rnh*B genes, was used as a host strain to overproduce the protein, to avoid contamination by RNases H1 and H2 from host cells [24]. *E. coli* MIC2067(DE3) transformants were grown at 30 °C in LB medium containing 30 mg·L^{-1} chloramphenicol and 50 mg·L^{-1} ampicillin. AaeRNH2 was overproduced and purified as described previously [49], except that *E. coli* MIC2067(DE3), instead of *E. coli* BL21(DE3), was used as a host strain. TmaRNH2 was overproduced and purified as described previously [49], with slight modifications. It was purified by two, instead of three, chromatographic procedures with a HiTrap SP column and a HiTrap Heparin column. These columns were equilibrated with 20 mM Tris/HCl (pH 8.0) containing 1 mM EDTA, instead of the same buffer without EDTA. The heat treatment was performed at 75 °C for 10 min, instead of 20 min, prior to these chromatographic procedures. TmaRNH2ΔC was overproduced and purified as described for TmaRNH2, except that the heat treatment and chromatography with a HiTrap SP column were not performed, and the gel filtration chromatography with a HiLoad 16/60 Superdex 200 pg column (GE Healthcare) equilibrated with 20 mM Tris/HCl (pH 8.0) containing 150 mM NaCl was performed at the end of the purification procedures. BstN–TmaRNH2ΔC was purified as described for TmaRNH2ΔC, except that the chromatography with a HiTrap Q HP column was performed at the beginning of the chromatographic procedures, and the concentration and pH of the Tris/HCl buffer were changed to 10 mM and pH 7.0, respectively.

BstRNH2 and BstRNH2ΔN were overproduced as described for TmaRNH2 and purified as described previously [36], except that the HiTrap Q HP and HiTrap Heparin columns were equilibrated with 10 mM Tris/HCl (pH 7.0), instead of 10 mM Tris/HCl (pH 7.5), containing 1 mM EDTA, and the two chromatographic procedures with a HiTrap SP column equilibrated with 10 mM Tris/HCl (pH 7.0) containing 1 mM EDTA and a HiLoad 16/60 Superdex 200 pg column equilibrated with 10 mM Tris/HCl (pH 7.0) containing 150 mM NaCl were performed at the end of the purification procedures.

The purity of the protein was analyzed by SDS/PAGE with a 15% polyacrylamide gel [51], followed by staining with Coomassie Brilliant Blue. The protein concentration was determined from UV absorption with $A_{280\ nm}$ values of a 0.1% solution (1.0 mg·mL^{-1}) of 0.88 cm^{-1} for AaeRNH2, 0.24 cm^{-1} for TmaRNH2, 0.30 cm^{-1} for TmaRNH2ΔC, 0.65 cm^{-1} for BstN–TmaRNH2ΔC, [illegible] cm^{-1} for BstRNH2, and 0.66 cm^{-1} for BstRNH2ΔN. These values were calculated by using absorption coefficients of 1576 M^{-1}·cm^{-1} for tyrosine and 5225 M^{-1}·cm^{-1} for tryptophan at 280 nm [52].

Enzymatic activity

The JRNase and RNase H activities were determined by using D15-R1-D13/D29 and R12/D12 as substrate, respectively. These substrates were prepared by hybridizing 1 μM 5′-fluorescence-labeled DNA_{15}-RNA_1-DNA_{13} (5′-AATAGAG[illegible]AAAGAAaAAAGATGGCAAAG-3′) and RNA_{12} (5′-cggagaugacgg-3′) with a 1.5 M equivalent of the complementary DNA, as described previously [50]. In these sequences, DNA and RNA are represented by uppercase and lowercase letters, respectively. All oligonucleotides were synthesized by Hokkaido System Science. The cleavage of the substrate at 30 °C for 15 min and separation of the products on a 20% polyacrylamide gel containing 7 M urea were carried out as described previously [50]. The products were detected with a Typhoon 9210 Imager (GE Healthcare), and quantified with IMAGEQUANT 5.2. One unit was defined as the amount of enzyme hydrolyzing 1 nmole of the substrate per minute at 30 °C. The specific activity was defined as the enzymatic activity per milligram of protein.

The reaction buffers were: 10 mM Tris/HCl (pH 8.0) containing 10 mM $MnCl_2$ or $MgCl_2$, 10 mM (for BstRNH2ΔN) or 50 mM (for BstRNH2) NaCl, 1 mM 2-mercaptoethanol and [illegible] μg·mL^{-1} BSA for BstRNH2 and BstRNH2ΔN; 15 mM Tris/HCl (pH 8.0) containing 1 mM $MnCl_2$ or $MgCl_2$, 50 mM NaCl, 1 mM dithiothreitol and 100 μg·mL^{-1} BSA for TmaRNH2, TmaRNH2ΔC, and BstN–TmaRNH2ΔC; and 20 Tris/HCl (pH 8.5) containing 10 mM $MnCl_2$ or $MgCl_2$, 100 mM KCl, 1 mM 2-mercaptoethanol and 100 μg·mL^{-1} BSA for AaeRNH2.

CD spectra

The far-UV (200–260 nm) CD spectra were measured on a J-725 spectropolarimeter (Japan Spectroscopic, Tokyo, Japan) at 25 °C. The protein was dissolved in 10 mM Tris/HCl (pH 8.0) at a concentration of ~ 0.1 mg·mL^{-1}. A cell with an optical path length of 2 mm was used. The mean residue ellipticity, θ, which has the units of deg cm^2·dmol^{-1}, was calculated by using a mean amino acid molecular mass of 110 Da.

Analysis of binding to substrate

Binding of the protein to the substrate was analyzed in the absence of the metal cofactor with a Biacore X instrument (Biacore, Uppsala, Sweden), as described previously [20], except that the substrate used to determine the JRNase activity (D15-R1-D13/D29) was immobilized on the sensor chip. The protein was dissolved in 10 mM Tris/HCl (pH 8.0) containing 50 mM NaCl, 1 mM 2-ME, 1 mM EDTA and 0.005% Tween P20 at various concentrations, and injected onto the sensor chip at 25 °C at a flow rate of 20 μL·min^{-1}. The binding surface was regenerated by washing with 2 M NaCl. The association constant K_A was estimated from the equilibrium levels of the protein binding to the surface as previously described [24].

Thermal denaturation

Thermal denaturation curves of the proteins were obtained by monitoring the change in CD values at 222 nm as the temperature was increased. The protein was dissolved in 10 mM Tris/HCl (pH 8.0) containing 1.5 M guanidine hydrochloride. The protein concentration and optical path length were 0.1 mg·mL^{-1} and 2 mm, respectively. The temperature of the protein solution was linearly increased by ~ 1.0 °C·min^{-1}. Thermal denaturation of these proteins was reversible under these conditions. The temperature of the midpoint of the transition, T_m, was calculated by curve fitting of the resultant CD values versus temperature data on the basis of a least-squares analysis.

3D modeling

A 3D model for the structures of AaeRNH2, BstRNH2ΔN and TmaRNH2ΔC was built with the SWISS-MODEL program [53], with the crystal structure of TmaRNH2 (PDB code 3O3F) as a template structure. Of various RNases H for which the crystal structures are available, TmaRNH2 shows the highest amino acid sequence identities with AaeRNH2 and BstRNH2, of 46.8% and 51.6%, respectively. A 3D model for the complex between TmaRNH2 and the D15-R1-D13/D29 substrate was built by using the programs COOT [54] and PYMOL (http://pymol.org), followed by energy minimization with GROMACS v. 4.5 [55]. The crystal structure of the TmaRNH2–substrate complex (PDB code 3O3F) was used as a template structure.

Acknowledgements

We thank J. Okada, N. Jongruja, T.-N. Nguyen, D.-J. You, H. Chon and K. Takano for helpful discussions. This work was supported in part by a grant (24380055) from the Ministry of Education, Culture, Sports, Science, and Technology of Japan.

References

1 Crouch RJ & Dirksen ML (1982) Ribonucleases H. In Nuclease (Linn SM & Roberts RJ, eds), pp. 211–241. Cold Spring Harbor Laboratory Press, Cold Spring Harbor, New York.

2 Nowotny M, Gaidamakov SA, Crouch RJ & Yang W (2005) Crystal structures of RNaseH bound to an RNA/DNA hybrid: substrate specificity and metal-dependent catalysis. *Cell* **121**, 1005–1016.

3 Nowotny M & Yang W (2006) Stepwise analyses of metal ions in RNase H catalysis from substrate destabilization to product release. *EMBO J* **25**, 1924–1933.

4 Yang W, Lee JY & Nowotny M (2006) Making and breaking nucleic acids: two-Mg^{2+}-ion catalysis and substrate specificity. *Mol Cell* **22**, 5–13.

5 Ohtani N, Haruki M, Morikawa M & Kanaya S (1999) Molecular diversities of RNases H. *J Biosci Bioeng* **88**, 12–19.

6 Nguyen TN, You DJ, Kanaya E, Koga Y & Kanaya S (2013) Crystal structure of metagenome-derived LC9-RNase H1 with atypical DEDN active site motif. *FEBS Lett* **587**, 1418–1423.

7 Tadokoro T & Kanaya S (2009) Ribonuclease H: molecular diversities, substrate binding domains, and catalytic mechanism of the prokaryotic enzymes. *FEBS J* **276**, 1482–1493.

8 Kogoma T & Foster PL (1998) Physiological functions of *E. coli* RNase HI. In Ribonucleases H (Crouch RJ & Toulme JJ, eds), pp. 39–66. INSERM, Paris.

9 Itaya M, Omori A, Kanaya S, Crouch RJ, Tanaka T & Kondo K (1999) Isolation of RNase H genes that are essential for growth of *Bacillus subtilis* 168. *J Bacteriol* **181**, 2118–2123.

10 Arudchandran A, Cerritelli S, Narimatsu S, Itaya M, Shin DY, Shimada Y & Crouch RJ (2000) The absence of ribonuclease H1 or H2 alters the sensitivity of *Saccharomyces cerevisiae* to hydroxyurea, caffeine and ethyl methanesulphonate: implications for roles of RNases H in DNA replication and repair. *Genes Cells* **5**, 789–802.

11 Cerritelli SM, Frolova EG, Feng C, Grinberg A, Love PE & Crouch RJ (2003) Failure to produce mitochondrial DNA results in embryonic lethality in Rnaseh1 null mice. *Mol Cell* **11**, 807–815.

12 Sparks JL, Chon H, Cerritelli SM, Kunkel TA, Johansson E, Crouch RJ & Burgers PM (2012) RNase H2-initiated ribonucleotide excision repair. *Mol Cell* **47**, 980–986.

13 Chon H, Sparks JL, Rychlik M, Nowotny M, Burgers PM, Crouch RJ & Cerritelli SM (2013) RNase H2 roles in genome integrity revealed by unlinking its activities. *Nucleic Acids Res* **41**, 3130–3143.

14 Reijns MA, Rabe B, Rigby RE, Mill P, Astell KR, Lettice LA, Boyle S, Leitch A, Keighren M, Kilanowski F *et al.* (2012) Enzymatic removal of ribonucleotides from DNA is essential for mammalian genome integrity and development. *Cell* **149**, 1008–1022.

15 Crow YJ, Leitch A, Hayward BE, Garner A, Parmar R & Jackson AP (2006) Mutations in genes encoding ribonuclease H2 subunits cause Aicardi–Goutieres syndrome and mimic congenital viral brain infection. *Nat Genet* **38**, 910–916.

16 Esposito F, Corona A & Tramontano E (2012) HIV-1 reverse transcriptase still remains a new drug target: structure, function, classical inhibitors, and new inhibitors with innovative mechanisms of actions. *Mol Biol Int* **2012**, 586401–586424.

17 Rychlik MP, Chon H, Cerritelli SM, Klimek P, Crouch RJ & Nowotny M (2010) Crystal structures of RNase H2 in complex with nucleic acid reveal the mechanism of RNA–DNA junction recognition and cleavage. *Mol Cell* **40**, 658–670.

18 Haruki M, Tsunaka Y, Morikawa M & Kanaya S (2002) Cleavage of a DNA–RNA–DNA/DNA chimeric substrate containing a single ribonucleotide at the DNA–RNA junction with prokaryotic RNases HII. *FEBS Lett* **531**, 204–208.

19 Rohman MS, Koga Y, Takano K, Chon H, Crouch RJ & Kanaya S (2008) Effect of the disease-causing mutations identified in human RNase H2 on the activities and stabilities of yeast RNase H2 and archaeal RNase HII. *FEBS J* **275**, 4836–4849.

20 Jongruja N, You DJ, Kanaya E, Koga Y, Takano K & Kanaya S (2010) The N-terminal hybrid binding domain of RNase HI from *Thermotoga maritima* is important for substrate binding and Mg^{2+}-dependent activity. *FEBS J* **277**, 4474–4489.

21 Tadokoro T, Chon H, Koga Y, Takano K & Kanaya S (2007) Identification of the gene encoding a type 1 RNase H with an N-terminal double-stranded RNA binding domain from a psychrotrophic bacterium. *FEBS J* **274**, 3715–3727.

22 Ohtani N, Tomita M & Itaya M (2008) Junction ribonuclease activity specified in RNases HII/2. *FEBS J* **275**, 5444–5455.

23 Ohtani N, Tomita M & Itaya M (2008) Junction ribonuclease: ribonuclease HII ortholog from *Thermus thermophilus* HB8 prefers RNA–DNA junction to RNA/DNA heteroduplex. *Biochem J* **412**, 517–526.

24 Jongruja N, You DJ, Angkawidjaja C, Kanaya E, Koga Y & Kanaya S (2012) Structure and characterization of RNase H3 from *Aquifex aeolicus*. *FEBS J* **279**, 2737–2753.

25 Lu Z, Liang R, Liu X, Hou J & Liu J (2012) RNase HIII from *Chlamydophila pneumoniae* can efficiently cleave double-stranded DNA carrying a chimeric ribonucleotide in the presence of manganese. *Mol Microbiol* **83**, 1080–1093.

26 Lu Z, Hou J, Wang Y & Liu J (2012) Involvement of Ser94 in RNase HIII from *Chlamydophila pneumoniae* in the recognition of a single ribonucleotide misincorporated into double-stranded DNA. *Biochim Biophys Acta* **1824**, 859–865.

27 Nowotny M, Gaidamakov SA, Ghirlando R, Cerritelli SM, Crouch RJ & Yang W (2007) Structure of human RNase H1 complexed with an RNA/DNA hybrid: insight into HIV reverse transcription. *Mol Cell* **28**, 513.

28 Nguyen TN, You DJ, Matsumoto H, Kanaya E, Koga Y & Kanaya S (2013) Crystal structure of metagenome-derived LC11-RNase H1 in complex with RNA/DNA hybrid. *J Struct Biol* **182**, 144–154.

29 Figiel M, Chon H, Cerritelli SM, Cybulska M, Crouch RJ & Nowotny M (2011) The structural and biochemical characterization of human RNase H2 complex reveals the molecular basis for substrate recognition and Aicardi–Goutieres syndrome defects. *J Biol Chem* **286**, 10540–10550.

30 Shaban NM, Harvey S, Perrino FW & Hollis T (2010) The structure of the mammalian RNase H2 complex provides insight into RNA·DNA hybrid processing to prevent immune dysfunction. *J Biol Chem* **285**, 3617–3624.

31 Reijns MA, Bubeck D, Gibson LC, Graham SC, Baillie GS, Jones EY & Jackson AP (2011) The structure of the human RNase H2 complex defines key interaction interfaces relevant to enzyme function and human disease. *J Biol Chem* **286**, 10530–10539.

32 Chon H, Matsumura H, Koga Y, Takano K & Kanaya S (2006) Crystal structure and structure-based mutational analyses of RNase HIII from *Bacillus stearothermophilus*: a new type 2 RNase H with TBP-like substrate-binding domain at the N terminus. *J Mol Biol* **356**, 165–178.

33 Deckert G, Warren PV, Gaasterland T, Young WG, Lenox AL, Graham DE, Overbeek R, Snead MA, Keller M, Aujay M *et al.* (1998) The complete genome of the hyperthermophilic bacterium *Aquifex aeolicus*. *Nature* **392**, 353–358.

34 Huber R, Langworthy TA, König H, Thomm M, Woese CR, Sleytr UB & Stetter KO (1986) *Thermotoga maritima* sp. nov. represents a new genus of unique extremely thermophilic eubacteria growing up to 90°C. *Arch Microbiol* **144**, 324–333.

35 Imanaka T, Fujii M, Aramori I & Aiba S (1982) Transformation of *Bacillus stearothermophilus* with plasmid DNA and characterization of shuttle vector plasmids between *Bacillus stearothermophilus* and *Bacillus subtilis*. *J Bacteriol* **149**, 824–830.

36 Muroya A, Nakano R, Ohtani N, Haruki M, Morikawa M & Kanaya S (2002) Importance of an N-terminal extension in ribonuclease HII from *Bacillus stearothermophilus* for substrate binding. *J Biosci Bioeng* **93**, 170–175.

37 Cerritelli SM & Crouch RJ (2009) Ribonuclease H: the enzymes in eukaryotes. *FEBS J* **276**, 1494–1505.

38 Hashimoto H, Inoue T, Nishioka M, Fujiwara S, Takagi M, Imanaka T & Kai Y (1999) Hyperthermostable protein structure maintained by intra and inter-helix ion pairs in archaeal O^6-methylguanine-DNA methyltransferase. *J Mol Biol* **292**, 707–716.

39 Karshikoff A & Ladenstein R (2001) Ion pairs and the thermotolerance of proteins from hyperthermophiles: a 'traffic rule' for hot roads. *Trends Biochem Sci* **26**, 550–556.

40 Uehara R, Takeuchi Y, Tanaka S, Takano K, Koga Y & Kanaya S (2012) Requirement of Ca^{2+} ions for the hyperthermostability of Tk-subtilisin from *Thermococcus kodakarensis*. *Biochemistry* **51**, 5369–5378.

41 Nguyen TN, Angkawidjaja C, Kanaya E, Koga Y, Takano K & Kanaya S (2012) Activity, stability, and structure of metagenome-derived LC11-RNase H1, a homolog of *Sulfolobus tokodaii* RNase H1. *Protein Sci* **21**, 553–561.

42 You DJ, Chon H, Koga Y, Takano K & Kanaya S (2007) Crystal structure of type 1 ribonuclease H from hyperthermophilic archaeon *Sulfolobus tokodaii*: role of Arg118 and C-terminal anchoring. *Biochemistry* **46**, 11494–11503.

43 Pace CN, Fu HL, Fryar KL, Landua J, Trevino SR, Shirley BA, Hendricks MM, Iimura S, Gajiwala K, Scholtz JM *et al.* (2011) Contribution of hydrophobic interactions to protein stability. *J Mol Biol* **408**, 514–528.

44 Thompson MJ & Eisenberg D (1999) Transproteomic evidence of a loop-deletion mechanism for enhancing protein thermostability. *J Mol Biol* **290**, 595–604.

45 Thoma R, Hennig M, Sterner R & Kirschner K (2000) Structure and function of mutationally generated monomers of dimeric phosphoribosylanthranilate isomerase from *Thermotoga maritima*. *Structure* **8**, 265–276.

46 Watanabe K, Chishiro K, Kitamura K & Suzuki Y (1991) Proline residues responsible for thermostability occur with high frequency in the loop regions of an extremely thermostable oligo-1,6-glucosidase from *Bacillus thermoglucosidasius* KP1006. *J Biol Chem* **266**, 24287–24294.

47 Boutz DR, Cascio D, Whitelegge J, Perry LJ & Yeates TO (2007) Discovery of a thermophilic protein complex stabilized by topologically interlinked chains. *J Mol Biol* **368**, 1332–1344.

48 Dundas J, Ouyang Z, Tseng J, Binkowski A, Turpaz Y & Liang J (2006) CASTp: computed atlas of surface topography of proteins with structural and topographical mapping of functionally annotated residues. *Nucleic Acids Res* **34**, W116–W118. (Web Server issue)

49 Okada J, Okamoto T, Mukaiyama A, Tadokoro T, You DJ, Chon H, Koga Y, Takano K & Kanaya S (2010) Evolution and thermodynamic of the slow unfolding of hyperstable monomeric proteins. *BMC Evol Biol* **10**, 207.
50 Ohtani N, Haruki M, Morikawa M, Crouch RJ, Itaya M & Kanaya S (1999) Identification of the genes encoding Mn^{2+}-dependent RNase HII and Mg^{2+}-dependent RNase HIII from *Bacillus subtilis*: classification of RNases H into three families. *Biochemistry* **38**, 605–618.
51 Laemmli UK (1970) Cleavage of structural proteins during the assembly of the head of bacteriophage T4. *Nature* **227**, 680–685.
52 Goodwin TW & Morton RA (1946) The spectrophotometric determination of tyrosine and tryptophan in proteins. *Biochem J* **40**, 628–632.
53 Schwede T, Kopp J, Guex N & Peitsch MC (2003) SWISS-MODEL: an automated protein homology-modeling server. *Nucleic Acids Res* **31**, 3381–3385.
54 Emsley P & Cowtan K (2004) Coot: model-building tools for molecular graphics. *Acta Crystallogr D Biol Crystallogr* **60**, 2126–2132.
55 Pronk S, Páll S, Schulz R, Larsson P, Bjelkmar P, Apostolov R, Shirts MR, Smith JC, Kasson PM, van der Spoel D *et al.* (2013) GROMACS 4.5: a high-throughput and highly parallel open source molecular simulation toolkit. *Bioinformatics* **29**, 845–854.

Supporting information

Additional supporting information may be found in the online version of this article at the publisher's web site:

Fig. S1. Alignment of the amino acid sequences of bacterial RNases H2.

Fig. S2. SDS/PAGE of the purified proteins.

Fig. S3. Stereoviews of the 3D models of AaeRNH2 and BstRNH2ΔN.

Etin Diah Permanasari, Ph.D, Apt.-Role of N-terminal extension of Bacillus stearothermophilus RNase H2 and C-terminal extension of Thermotoga maritima RNase H2

ORIGINALITY REPORT

22%	12%	21%	4%
SIMILARITY INDEX	INTERNET SOURCES	PUBLICATIONS	STUDENT PAPERS

PRIMARY SOURCES

1	Elias Tannous, Koji Yokoyama, Dong-Ju You, Yuichi Koga, Shigenori Kanaya. " A dual role of divalent metal ions in catalysis and folding of RNase H1 from extreme halophilic archaeon sp. NRC-1 ", FEBS Open Bio, 2012 Publication	2%
2	Takashi Tadokoro, Dong-Ju You, Yumi Abe, Hyongi Chon, Hiroyoshi Matsumura, Yuichi Koga, Kazufumi Takano, Shigenori Kanaya. " Structural, Thermodynamic, and Mutational Analyses of a Psychrotrophic RNase HI ", Biochemistry, 2007 Publication	1%
3	Sulaiman, Sintawee, Dong-Ju You, Eiko Kanaya, Yuichi Koga, and Shigenori Kanaya. "Crystal Structure and Thermodynamic and Kinetic Stability of Metagenome-Derived LC-Cutinase", Biochemistry, 2014. Publication	1%

4	Okano, Hiroyuki, Masashi Ozaki, Eiko Kanaya, Joong-Jae Kim, Clement Angkawidjaja, Yuichi Koga, and Shigenori Kanaya. "Structure and stability of metagenome-derived glycoside hydrolase family 12 cellulase (LC-CelA) a homolog of Cel12A from Rhodothermus marinus", FEBS Open Bio, 2014. Publication	1%
5	You, Dong-Ju, Hyongi Chon, Yuichi Koga, Kazufumi Takano, and Shigenori Kanaya. "Crystal Structure of Type 1 Ribonuclease H from Hyperthermophilic Archaeon *Sulfolobus tokodaii*: Role of Arginine 118 and C-Terminal Anchoring†,‡", Biochemistry, 2007. Publication	1%
6	Chon, H.. "Crystal Structure and Structure-based Mutational Analyses of RNase HIII from Bacillus stearothermophilus: A New Type 2 RNase H with TBP-like Substrate-binding Domain at the N Terminus", Journal of Molecular Biology, 20060210 Publication	1%
7	Submitted to Parkland College Student Paper	1%
8	Dong-Ju You, Nujarin Jongruja, Elias Tannous, Clement Angkawidjaja, Yuichi Koga, Shigenori Kanaya. "Structural basis for salt-dependent	1%

folding of ribonuclease H1 from halophilic archaeon Halobacterium sp. NRC-1", Journal of Structural Biology, 2014
Publication

9	Submitted to University of Westminster Student Paper	1%
10	Tri-Nhan Nguyen, Dong-Ju You, Eiko Kanaya, Yuichi Koga, Shigenori Kanaya. "Crystal structure of metagenome-derived LC9-RNase H1 with atypical DEDN active site motif", FEBS Letters, 2013 Publication	1%
11	ir.library.osaka-u.ac.jp Internet Source	1%
12	Tri-Nhan Nguyen. "Activity, stability, and structure of metagenome-derived LC11-RNase H1, a homolog of Sulfolobus tokodaii RNase H1", Protein Science, 04/2012 Publication	1%
13	www.deepdyve.com Internet Source	1%
14	Ohtani, Naoto, Mitsuru Haruki, Masaaki Morikawa, Robert J. Crouch, Mitsuhiro Itaya, and Shigenori Kanaya. "Identification of the Genes Encoding Mn^{2+}-Dependent RNase HII and Mg^{2+}-Dependent RNase HIII from *Bacillus*	1%

subtilis: Classification of RNases H into Three Families†", Biochemistry, 1999.
Publication

---

15 Takashi Tadokoro, Kyoko Matsushita, Yumi Abe, Muhammad Saifur Rohman, Yuichi Koga, Kazufumi Takano, Shigenori Kanaya. " Remarkable Stabilization of a Psychrotrophic RNase HI by a Combination of Thermostabilizing Mutations Identified by the Suppressor Mutation Method ", Biochemistry, 2008 — 1%
Publication

---

16 Rychlik, M.P.. "Crystal Structures of RNase H2 in Complex with Nucleic Acid Reveal the Mechanism of RNA-DNA Junction Recognition and Cleavage", Molecular Cell, 20101124 — 1%
Publication

---

17 aem.asm.org — 1%
Internet Source

---

18 CHON, Hyongi, Rikita NAKANO, Naoto OHTANI, Mitsuru HARUKI, Kazufumi TAKANO, Masaaki MORIKAWA, and Shigenori KANAYA. "Gene Cloning and Biochemical Characterizations of Thermostable Ribonuclease HIII from Bacillus stearothermophilus", Bioscience Biotechnology and Biochemistry, 2004. — 1%

Publication

19	peds.oupjournals.org Internet Source	<1%
20	Tannous, Elias, Koji Yokoyama, Dong-Ju You, Yuichi Koga, and Shigenori Kanaya. "A dual role of divalent metal ions in catalysis and folding of RNase H1 from extreme halophilic archaeon Halobacterium sp. NRC-1", FEBS Open Bio, 2012. Publication	<1%
21	Foophow, T.. "Crystal Structure of a Subtilisin Homologue, Tk-SP, from Thermococcus kodakaraensis: Requirement of a C-terminal @b-Jelly Roll Domain for Hyperstability", Journal of Molecular Biology, 20100723 Publication	<1%
22	Uehara, Ryo, Clement Angkawidjaja, Yuichi Koga, and Shigenori Kanaya. "Formation of the High-Affinity Calcium Binding Site in Pro-subtilisin E with the Insertion Sequence IS1 of Pro-Tk-subtilisin", Biochemistry, 2013. Publication	<1%
23	K. Kuwahara. "Importance of an extreme C-terminal motif of a family I.3 lipase for stability", Protein Engineering Design and Selection, 05/01/2011 Publication	<1%

24	Cheng, M., C. Angkawidjaja, Y. Koga, and S. Kanaya. "Calcium-independent opening of lid1 of a family I.3 lipase by a single Asp to Arg mutation at the calcium-binding site", Protein Engineering Design and Selection, 2014. Publication	<1%
25	abbs.oxfordjournals.org Internet Source	<1%
26	pubmedcentralcanada.ca Internet Source	<1%
27	peds.oxfordjournals.org Internet Source	<1%
28	Naoto Ohtani. "The SCO2299 gene from Streptomyces coelicolor A3(2) encodes a bifunctional enzyme consisting of an RNase H domain and an acid phosphatase domain", FEBS Journal, 6/2005 Publication	<1%
29	Atsuko Akasako, Mitsuru Haruki, Motohisa Oobatake, Shigenori Kanaya. " Conformational Stabilities of RNase HI Variants with a Series of Amino Acid Substitutions at a Cavity within the Hydrophobic Core ", Journal of Biological Chemistry, 1997 Publication	<1%
30	Shigenori Kanaya. "Prokaryotic Type 2 RNases	<1%

H", Elsevier BV, 2001
Publication

31	Yasuo Tsunaka, Mitsuru Haruki, Masaaki Morikawa, Motohisa Oobatake, Shigenori Kanaya. " Dispensability of Glutamic Acid 48 and Aspartic Acid 134 for Mn -Dependent Activity of Ribonuclease HI ", Biochemistry, 2003 Publication	<1%
32	www.biochemj.org Internet Source	<1%
33	Submitted to University of Queensland Student Paper	<1%
34	Busti, P.. "Thermal unfolding of bovine @b-lactoglobulin studied by UV spectroscopy and fluorescence quenching", Food Research International, 200506 Publication	<1%
35	Andrey Karshikoff, Rudolf Ladenstein. "Ion pairs and the thermotolerance of proteins from hyperthermophiles: a ‘traffic rule’ for hot roads", Trends in Biochemical Sciences, 2001 Publication	<1%

Exclude quotes On Exclude matches < 17 words

Exclude bibliography On